

Modelling and identification of coupled thermo-viscoplastic material behaviour with nonlocal ductile damage

Marvin Nahrman¹, Anton Matzenmiller^{1,2}

¹Institute of Mechanics, Department of Mechanical Engineering, University of Kassel,
Mönchebergstr. 7, 34125 Kassel, Germany

²Professor of Applied Mechanics

Abstract

The postcritical behaviour due to mechanical loading of the high strength steel HX340LAD (ZStE340), typically used for cold forming of complex structures is modelled by means of a yield curve in the softening part of the material. Due to local heating, caused by viscoplastic deformations particularly for high strain rates, a thermo-mechanical coupled simulation is carried out by taking into account the conversion of plastic work into heat. Moreover, a temperature and rate dependent material model, coupled with ductile damage, is applied to allow the prediction of damage and failure of metal components caused by large plastic deformations during forging or sheet metal forming. The constitutive equations are implemented as a user defined material model into LS-DYNA and include the temperature dependency of the material parameters such as for the YOUNG's modulus, the initial yield stress, the nonlinear isotropic hardening parameter, the strain rate sensitivity as well as for the moduli of a continuum damage mechanics based approach. The nonlocal damage option ***MAT_NONLOCAL** in LS-DYNA is used to prevent localisation of the damaged zone for small elements. Test data of tensile specimens are considered under different strain rates from 0.006 1/s (quasistatic) up to 100 1/s for identifying the model parameters with the optimisation software LS-OPT. Finally, the numerically predicted stress-strain curves are compared to the according test data for the model verification. In addition, the computed heat evolution due to plastic flow is compared to the experimental measured data in terms of time-temperature courses. Finally, the plastic necking of the tensile specimen is investigated by means of the spatial strain distribution.

Keywords

thermo-viscoplasticity, nonlocal ductile damage, high strength steel

1 Introduction

Modern lightweight car body structures consist of a broad variety of different materials such as different types of aluminium and steel alloys as well as carbon fibre reinforced plastics. Different material properties are the reasons for this diversity, beneficially utilised for different vehicle components ensuring the occupant safety. In case of steel alloys, a compromise between material strength and ductility must be made. Microalloyed steels (HSLA steels) show a high yield and tensile strength, thus they are suited for complex cold-formed car body structures.

Due to the tremendous effort for experimental tests, computer based simulations are frequently integrated into the development process. Thereby, the thermo-mechanical material behaviour has to be considered, due to the conversion of plastic work into heat during metal forming, particularly for high strain rates. The precise prediction of the damage state is of high interest recognising manufacturing defects in an early development stage. Moreover, undetected damage can undesirably influence the probabilities of the component produced.

For the finite element (FE) simulation of metal forming processes, suitable material models are necessary including temperature and strain rate dependent plasticity as well as damage up to fracture. In this contribution, a thermo-viscoplastic material model is coupled with a ductile damage approach based on continuum damage mechanics. Moreover, the nonlocal formulation of the damage variable is applied by means of the keyword `*MAT_NONLOCAL` in the FE-code LS-DYNA, Rev. 10.0.0.

2 Thermo-viscoplastic material model

The constitutive equations of the thermo-viscoplastic material model based on [1], [2] and [3] have been implemented as a user defined material model into LS-DYNA—see [9] and [10]—obtaining temperature and strain rate dependent material behaviour. Therefore, the temperature dependency of the material parameters such as for the YOUNG's modulus, the initial yield stress, the nonlinear isotropic hardening parameter and the strain rate sensitivity are taken into account. Originally, the material model is developed for the simulation of simultaneous hot/cold forging processes with a large temperature range from room temperature to nearly up to the melting point—see [4] and [5]. However, it can be also used additionally in the small range near room temperature as for the example in this contribution.

The thermo-elastic material behaviour is considered by means of the temperature dependent YOUNG's modulus, leading to the temperature dependency of the bulk $\hat{K}(\theta)$ and shear modulus $\hat{G}(\theta)$ of linear elasticity.

$$\mathbf{T} = 2 \hat{G}(\theta) \mathbf{E}_{el}^D + 3 \hat{K}(\theta) \mathbf{E}_{el}^V \quad (1)$$

The CAUCHY stress tensor is denoted as \mathbf{T} and the deviatoric and volumetric part of the elastic strain tensor as \mathbf{E}_{el}^D and \mathbf{E}_{el}^V respectively. A hyperbolic tangent function with three parameters is applied for temperature dependent function of the YOUNG's modulus $\hat{E}(\theta)$ decreasing with rising absolute temperature θ —see

$$\hat{E}(\theta) = \frac{1}{2} E \left(1 + \tanh(Q_E(\theta_E - \theta)) \right) \quad (2)$$

This function is well suited for the large temperature range appearing in simultaneous hot/cold forming processes, however, choosing a small value for Q_E leads to a simple, almost linear functional dependency in the case of small temperature changes as considered in this contribution. The VON MISES yield criterion

$$F = \sqrt{3J_2} - (\hat{\kappa}_0(\theta) + \kappa(\theta)) \stackrel{!}{=} 0 \quad (3)$$

distinguishes between elastic and viscoplastic deformations in metals, whereby J_2 is the second invariant of the deviatoric stress tensor and $\sigma_{eq} = \sqrt{3J_2}$ is the VON MISES equivalent stress. The temperature dependent approach for the initial yield stress

$$\hat{\kappa}_0(\theta) = \frac{1}{2} \kappa_0 \left(1 + \tanh(Q_{\kappa_0}(\theta_{\kappa_0} - \theta)) \right) \quad (4)$$

is basically identical to the one for the YOUNG's modulus—see also Fig. 1 (a). The nonlinear isotropic hardening is obtained with the ansatz:

$$\kappa = \kappa^\infty \left[1 - \exp\left(-\frac{E_\kappa}{\kappa^\infty} \bar{E}_{vp}\right) + \frac{E^\infty}{\kappa^\infty} \bar{E}_{vp} \right] \quad (5)$$

It is driven by the equivalent viscoplastic strain denoted as \bar{E}_{vp} . The plastic hardening description is set up by means of a saturating exponential function and a linear term, whereby all three parameters are necessary—see Fig.1 (b). In addition, the hardening modulus E^∞ is temperature and strain rate dependent through the function

$$\hat{E}^\infty(\theta, \dot{\bar{E}}) = E^\infty \left[1 - \langle \theta - \theta_0 \rangle (\alpha_{\kappa\theta} + \alpha_{\kappa\dot{\bar{E}}} \langle \ln \frac{\dot{\bar{E}}}{\dot{\bar{E}}_0} \rangle) \right] \quad (6)$$

reducing the hardening slope with increasing temperature and strain rate. The function contains the reference temperature θ_0 and the reference strain rate $\dot{\bar{E}}_0$ as well as the two model parameters $\alpha_{\kappa\theta}$ and $\alpha_{\kappa\dot{\bar{E}}}$ that are identified with temperature and strain rate dependent test data, respectively. The application of the Macauley brackets $\langle \dots \rangle$ leads to a zero value for negative arguments, i. e. for temperatures or strain rates below their reference values.

In the case of $F > 0$, the viscoplastic deformations are determined by the associated flow rule (normality rule).

$$\dot{\bar{E}}_{vp} = \lambda \mathbf{N}(\mathbf{T}^D) = \lambda \frac{\mathbf{T}^D}{\|\mathbf{T}^D\|}, \quad \lambda = \frac{1}{\eta} \left\langle \frac{F}{D_0} \right\rangle^m, \quad (7)$$

with the variable $\dot{\bar{E}}_{vp}$ as the rate of the viscoplastic strain tensor and \mathbf{T}^D as the deviatoric part of the CAUCHY stress. The strain rate dependent material behaviour is obtained by means of a PERZYNA type approach for the viscoplastic multiplier λ , which contains the two parameters η and m as well as the normalisation factor D_0 . The pre-factor η can be interpreted as pseudo-viscosity and the inverse of the exponent m is the gradient in a double logarithmic scale and determines the nonlinearity of the strain rate sensitivity—see Fig. 1 (c).

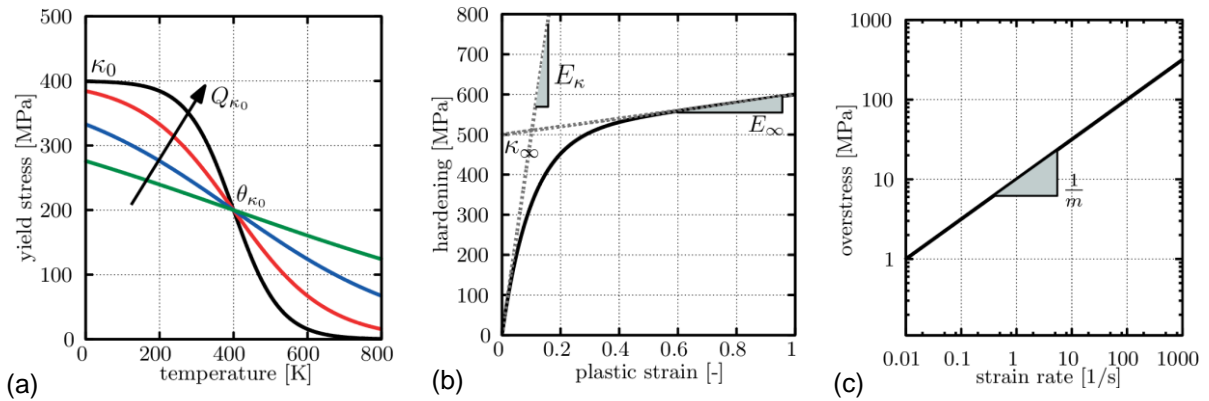


Fig.1: Schematic plots of material behavior: temperature dependent yield stress (a), nonlinear isotropic hardening (b), nonlinear strain rate sensitivity (c)

During metal forming, local heating is caused by viscoplastic deformations leading to a significant temperature rise, particularly for loadings under high strain rates. Hence, the conversion of the dissipated work into heat is taken into account by means of the TAYLOR-QUINNEY approach (see [6])

$$\dot{\theta} = \frac{\gamma_{TQ}}{\rho c_v} \mathbf{T} \cdot \dot{\bar{E}}_{vp}, \quad \gamma_{TQ} = 0.90 \quad (8)$$

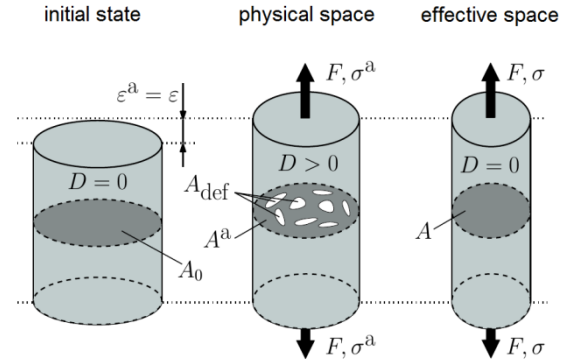
with a value of 0.90 for the related coefficient meaning that 90 % of the viscoplastic work are dissipated into heat energy. Moreover, the density ρ and the specific heat capacity c_v appear in the TAYLOR-QUINNEY assumption. The consequence of the mutual interaction of the temperature and displacement field is a thermo-mechanically coupled problem, solved by means of the staggered solution scheme in LS-DYNA. Hence, during the solution of the mechanical problem fixed temperatures are supposed and the thermal problem is solved with fixed displacements. The thermal and the mechanical time step size can be taken differently, depending on the necessities of the thermo-mechanical problem considered.

3 Modelling of nonlocal ductile damage

The void growth due to plasticity in the ductile high strength steel alloy HX340LAD is modelled by means of the theory of continuum damage mechanics, where a scalar variable D is sufficient to model isotropic damage behaviour. The damage variable can be interpreted as the ratio of the area of defects A_{def} to the total area A^a (see Fig. 2) and has a value of $D = 0$ at the initial state. It emerges with increasing plastic deformations up to its maximum at $D = 1$ in case of a totally damaged material.

$$D = \frac{A_{\text{def}}}{A^a}, \quad 0 \leq D < 1$$

(9) Fig.2: Concept of effective stresses



The constitutive equations of the thermo-viscoplastic material model (Eq. 1–7) are coupled with the damage approach by means of the concept of effective stresses depicted in Fig. 2—see [12] and the cited references therein. The uniaxial stress in the physical space (damaged configuration) $\sigma^a = F / A^a$ and in the effective one (undamaged configuration) $\sigma = F / A$ with $A = A^a - A_{\text{def}}$ are related by $\sigma^a = \sigma (1 - D)$. Transferred to the three-dimensional state, the CAUCHY stress tensor in the physical space \mathbf{T}^a is obtained from the stress tensor in the effective space \mathbf{T} becomes

$$\mathbf{T}^a = (1 - D) \mathbf{T} \quad (10)$$

Due to the strain equivalence principle, the strains in the physical ε^a and the effective space ε shall be identical, leading to equivalent internal strains as well—see [7] and [8]. For the purpose of ductile damage evolution, the approach, proposed by LEMAITRE [11], is considered here:

$$D = \left\langle \frac{\bar{E}_{\text{vp}} - \varepsilon_{c0}}{\varepsilon_{f0} - \varepsilon_{c0}} \right\rangle^{n_D} \quad (11)$$

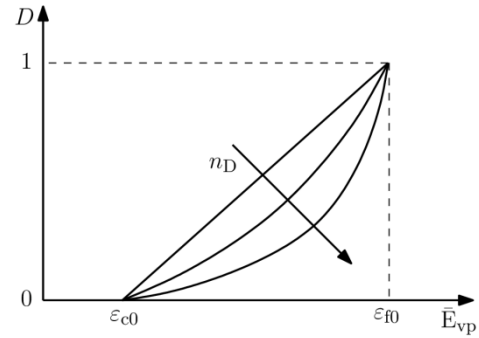


Fig.3: Influence of the damage exponent on damage accumulation

The damage evolution starts when the equivalent viscoplastic strain \bar{E}_{vp} passes its critical value of ε_{c0} and results in failure by reaching the final strain limit ε_{f0} . Both, the critical and the failure strain are model parameters and depend on steel type investigated. Moreover, the exponent n_D controls the accumulation of damage, whereby $n_D = 1$ means linear damage growth and $n_D \geq 2$ implies a nonlinear damage accumulation—see Fig. 3. The influence of multiaxial loading, temperature and strain rate sensitivity to the damage behaviour is widely modelled with the help of the JOHNSON-COOK assumption [13]:

$$\varepsilon_f = \left(d_1 + d_2 e^{-d_3 T} \right) \left(1 + d_4 \ln \frac{\dot{E}_{\text{vp}}}{\dot{\varepsilon}_0} \right) (1 + d_5 \theta^*), \quad \theta^* = \frac{\theta - \theta_0}{\theta_m - \theta_0} \quad (12)$$

Thereby, multiaxial loading is considered by the stress triaxiality $T = \frac{\sigma_m}{\sigma_{\text{eq}}}$ as the hydrostatic stress $\sigma_m = \frac{1}{3} I_1$ with respect to the VON MISES equivalent stress σ_{eq} with I_1 is the first invariant of the CAUCHY stress tensor \mathbf{T} . A more sophisticated failure approach is proposed by BAO and WIERZBICKI in [14] and [15] for modelling the stress state dependent failure of the aluminium alloy Al 2024-T351, whereby a function is defined in three sections of the stress triaxiality. In [16], SUN et al. propose a failure model for the stress state dependent failure modelling of TRIP steel differentiating between two regions of the stress triaxiality in order to regard two different failure mechanisms, i.e. dimple rupture and shear failure. In addition to the triaxiality, a further stress invariant is necessary to describe failure, caused by the three-dimensional stress state: For this, the LODE parameter is an appropriate choice including the third invariant of the stress deviator—see [15]. However, instead of a stress state dependent damage model, the different damage mechanisms under hydrostatic tension and due to shear dominated stress state (see Fig. 4) are considered by means of different critical strain values ε_{c0} and failure parameters ε_{f0} for tension and shear in this paper.

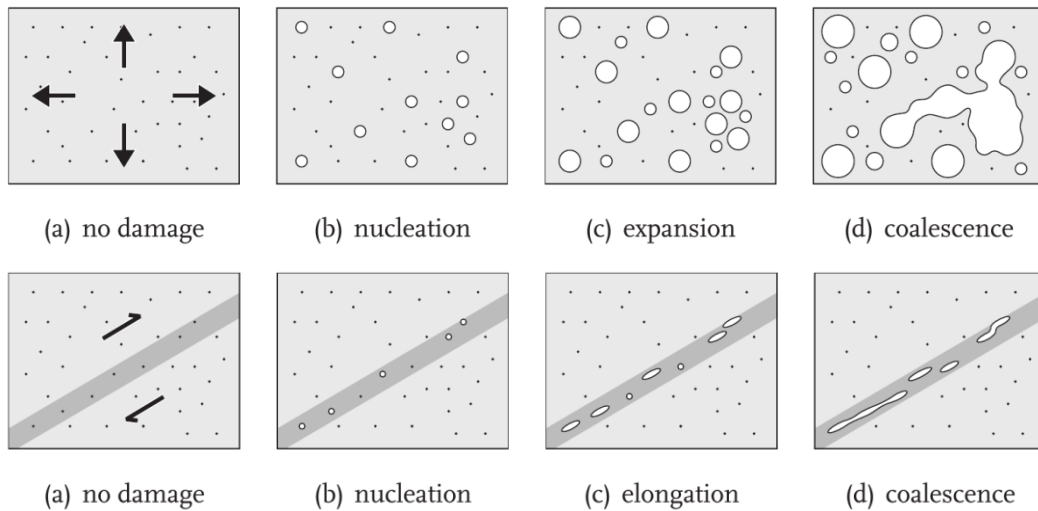


Fig.4: Schematic representation of different damage mechanisms under hydrostatic tension (upper row) and shear dominated stress (lower row) [21, p. 81]

In order to prevent the localisation of the spatial damage field, the nonlocal damage option in LS-DYNA is used by means of the keyword ***MAT_NONLOCAL**. This formulation is based on the work [17] and applied for simulation of a metal forming process in [18] and with failure of aluminum under impact loading in [19]. The theory behind ***MAT_NONLOCAL** is comprehensively explained in [20], and briefly recaptured in the following.

The variable for nonlocal damage is obtained by weighting and integration of the local damage field related to the element e_r over the area Ω_r —see Fig. 5 (a). Thereby, the size of the integration area is determined by the characteristic length L that represents the damage zone and has to be estimated by experimental experience. For the averaging of the local damage, the weighting function

$$w_{r,i} = w(x_r - y_i) = \left[1 + \left(\frac{\|x_r - y_i\|}{L} \right)^p \right]^{-q} \quad (13)$$

is defined by with the distance $\|x_r - y_i\|$ of the reference point x_r in element e_r to the point y_i in an arbitrary element of the integration area with respect to the characteristic length L in its argument together with the two parameters p and q specifying its shape. A comparison of different values for p and q is shown in Fig. 5 (b) and (c), whereby typical values are $q=2$ and $p=8$ resulting in a broad localisation zone and a rapid decrease.

The different damage mechanisms lead to different sizes of the damage zone, whereby in case of the hydrostatic tension, a broad zone of damaged material occurs, whereas a localised shear band leads to failure in the case of shear dominated stress state—see Fig. 4. Therefore, different characteristic length scales L of the nonlocal damage model have to be applied for the simulation of hydrostatic tension and shear dominated stress states, respectively.

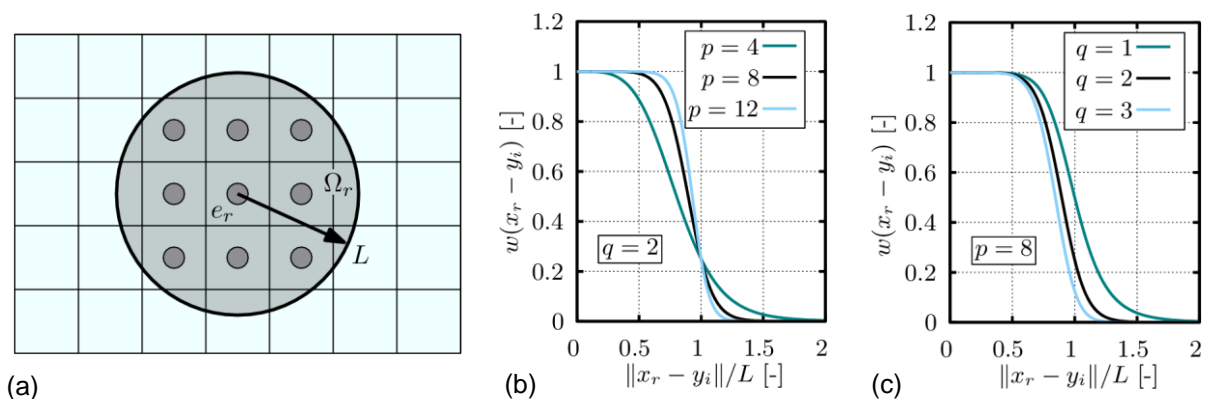


Fig.5: Nonlocal damage model in LS-DYNA according to [20]

4 Parameter identification and model verification

A step-by-step identification strategy is pursued for the identification of the model parameters. First, the rate- and temperature-independent coefficients are identified by using quasistatic tensile and shear tests at room temperature. The test data are used up to the maximum of strength excluding the data at necking process of the specimens for the identification of the initial yield stress and the parameters for the isotropic hardening formulation. The local heating, as a result of plastic deformations, has only a little effect on the temperature rise, due to the extensive heat conduction during the comparably long testing interval. It is assumed that the effect of strain rate sensitivity can be neglected in quasistatic tests, although local strain rates could be higher than the one prescribed. All model parameters are identified by means of fitting the simulation results to the test data by using the optimisation software LS-OPT [26]. The deviation of both courses is evaluated on the basis of the mean squared error (MSE), calculated and minimised during the optimisation procedure.

The FE models of the tensile and the shear specimen are depicted in Fig. 6 together with the geometric data and the boundary conditions. Due to symmetry, only one half of the tensile specimen is modelled for the simulation, where symmetric boundary conditions are introduced. The upper clamping is accounted for by means of a rigid body that is only moveable in y -direction. The lower clamping is also modelled as rigid and it is fixed in all degrees of freedom. The load is applied by a smooth ramp for the velocity-time graph up to a constant value in order to avoid strong accelerations at early stage. A cross section plane is introduced for evaluating the force in y -direction. The local displacements are obtained from the displacement differences in y -direction of the two marked locations in Fig. 6 in accordance with the experimental setup. The nominal strain is calculated by the ratio of the length change and the initial length, which is 25 mm in case of the tensile specimen and 30 mm for the shear specimen respectively. In order to analyse the nominal stress, the evaluated force in the cross section plane is divided by the cross section area, which is 15 mm^2 ($1.5 \text{ mm} \times 10 \text{ mm}$) for the full tensile specimen and 10.7 mm^2 ($1.5 \text{ mm} \times 7.13 \text{ mm}$) in the case of the shear specimen—see also [23, p. 40]. The element size in the damage zone of the tensile specimen is $0.5 \text{ mm} \times 0.7 \text{ mm}$ and $0.4 \text{ mm} \times 0.5 \text{ mm}$ for the shear test body respectively. Both specimens are modelled with four elements in thickness direction resulting in a minimal element size of 0.375 mm .

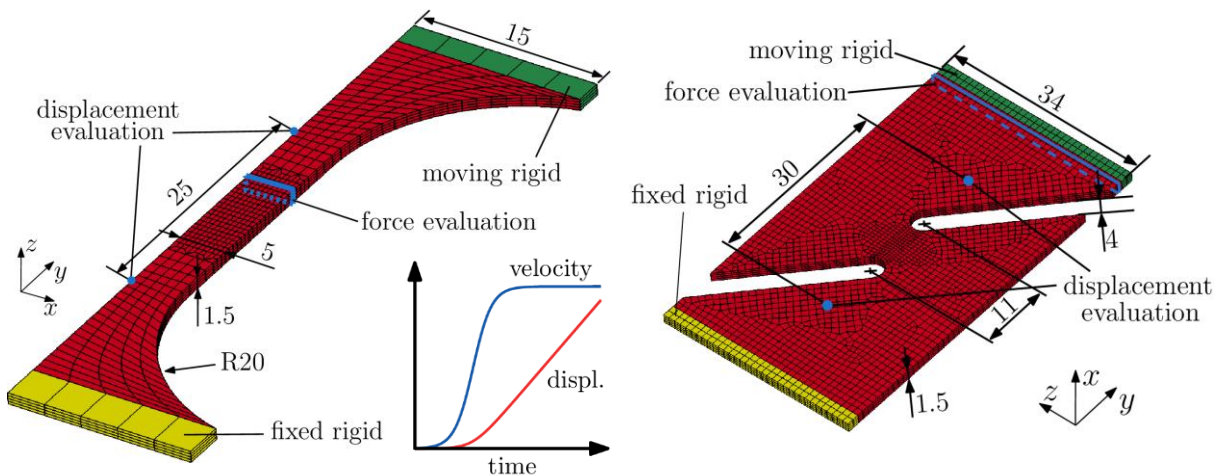


Fig.6: FE models of the tensile specimen (left) and the shear specimen (right) with boundary conditions and geometric measurements

Different pairs of the damage model parameters ε_{c0} and ε_{f0} are obtained for each simulation of the both loading cases—see table in Fig. 7. Moreover, the characteristic length L for the option of nonlocal damage is chosen differently due to the various damage mechanisms. A significantly smaller value is taken for the shear band localisation—see Fig. 4. The comparison of the predicted stress-strain courses of the tensile and shear test with the according test data in Fig. 7 shows a very good agreement for both loading scenarios. Based on these results, it can be concluded that the pressure independent yield theory according to VON MISES as well as the chosen isotropic hardening approach is accurate enough for the model of this specific steel alloy. However, it should be mentioned that some metals are pressure sensitive regarding plasticity—see also [15].

The different damage mechanisms for tensile and shear loading are reflected by the simulation results considering the equivalent plastic strain as well as the damage variable. A large plastic zone appears

in the case of the tensile specimen resulting in a pronounced damage zone—see Fig. 8, upper row. Consequently, damage evolution remains in the broad neighbourhood of failed elements. The plastic zone of the shear specimen is significantly smaller than the one in the tensile specimen and is leading to a narrow damage zone that almost only arises in the area of failure—see Fig. 8, lower row. The predicted points of failure at the maximum of the damage variable and the deformed specimen after failure (see [24, p. 77]) are in very good accordance with the test results.

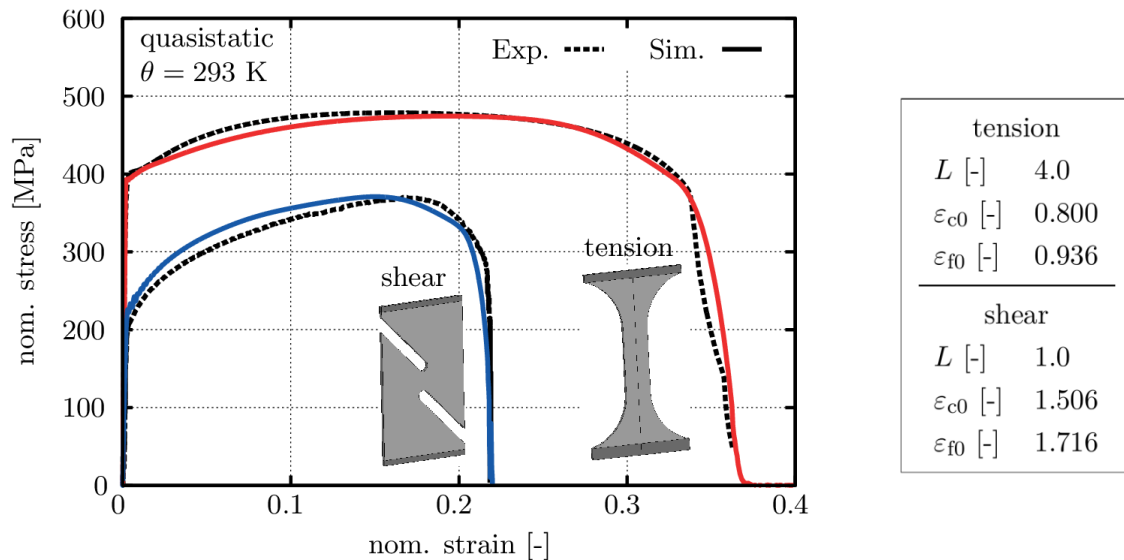


Fig.7: Experimental data of the tension test from [22] and shear test from [23] compared to the simulation results obtained with the according parameters of the nonlocal damage model

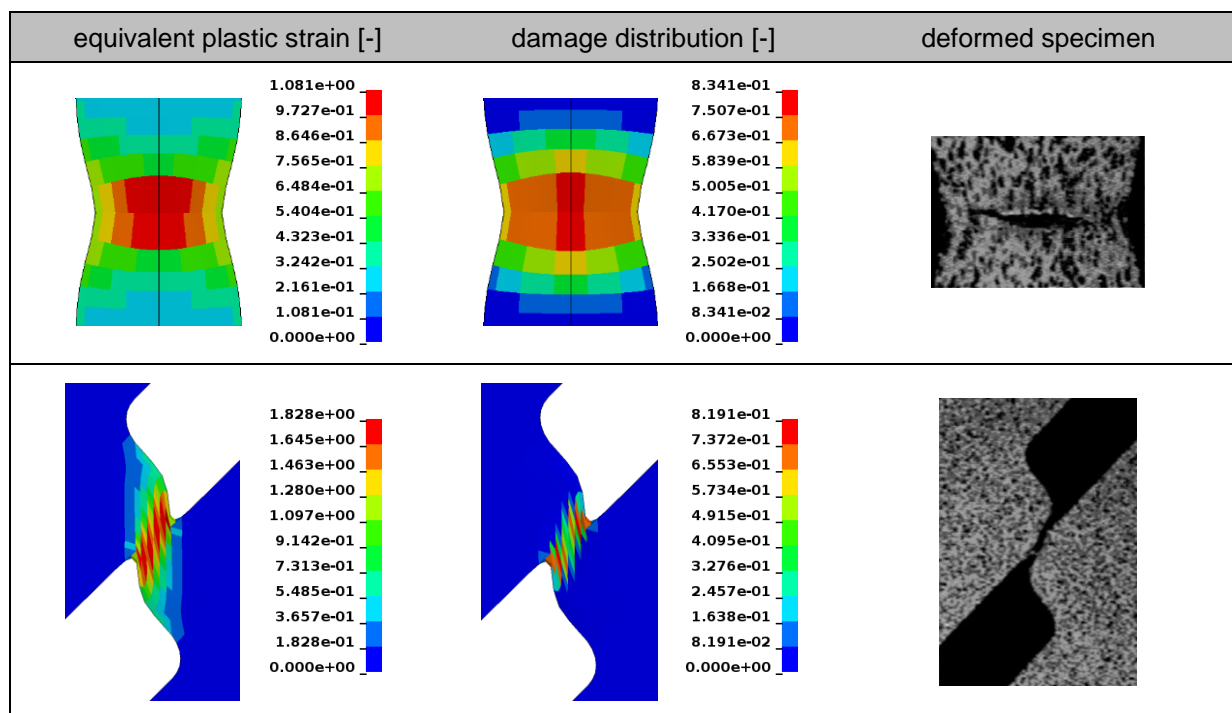


Fig.8: Fringe plot of the equivalent plastic strain and the damage variable shortly before fracture compared to the deformed specimen after failure from [24, p. 77] for the tensile specimen (upper row) and shear specimen (lower row of figures)

Because of the nearly adiabatic heating conditions for high strain rate tests, the temperature dependent material behaviour is analysed first. Due to the lack of test data, only quasistatic stress-strain courses with temperature values from 20 °C (293 K) up to 200 °C (473 K) are considered. Hence, the parameters for the temperature dependent YOUNG's modulus (Eq. 2), the initial yield stress (Eq. 4) and the isotropic hardening (Eq. 6) are identified with the test data taken from [24, p. 63–64]. All identified model parameters are listed in Tab. 1.

The simulation results closely match the test data in Fig. 9 for the case of 100 °C (373 K). A mediocre accordance is found for 200 °C (473 K). Consequently, the material model and the identified parameters are verified for temperature dependent applications.

The strain rate dependent simulation results are compared to the related test data from [22] and [23] in Fig. 10, whereby the already discussed quasistatic outcome is depicted additionally to the strain rates of 1 s⁻¹, 10 s⁻¹ and 100 s⁻¹. The overall agreement of measured and predicted stress-strain curves is good. Particularly, the initial yield stress and the initial hardening of the simulations and the test data are in very good correlation for each loading condition and demonstrate the prediction capability of the material model before necking of the specimen occurs. After reaching the ultimate tensile strength at maximal stress, necking of the specimen arises and leads to an inhomogeneous stress state. Additionally, the temperature increase and damage growth in the necking area make the prediction of the material behaviour in the post-necking area to a most challenging object of tensile test simulation. Here, the prediction accuracy of the material model at the medium strain rate 1 s⁻¹ is very good regarding the stress-strain course. However, the accordance of simulation results and test data is reduced with increasing strain rate.

The equivalent strain centrally measured in the necking area before fracture (see [23, p. 119]), is compared to the predicted equivalent strain in Fig. 10, whereby the predicted equivalent strain is evaluated before the damage variable reaches its final value of $D = 1$. The test data and the simulation results agree well for all investigated strain rates and predict the material behaviour accurately, although the strain maximum and the width of the plastic zone are slightly overestimated.

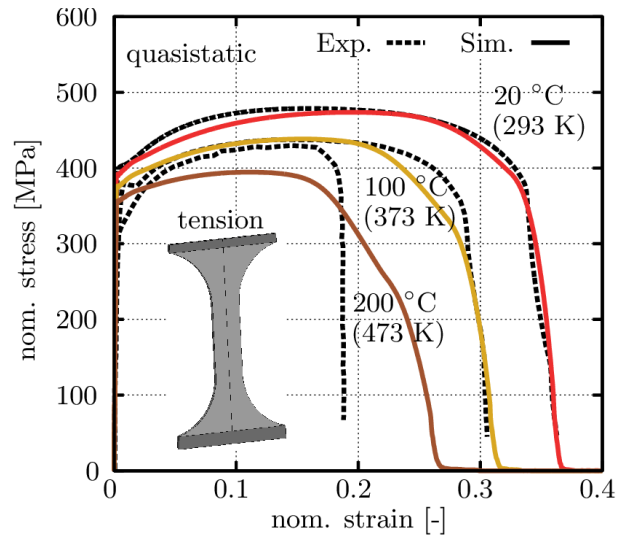


Fig.9: Experimental data of the tension test at 293 K from [22] and at 373 K as well as 473 K from [24] compared with the simulation

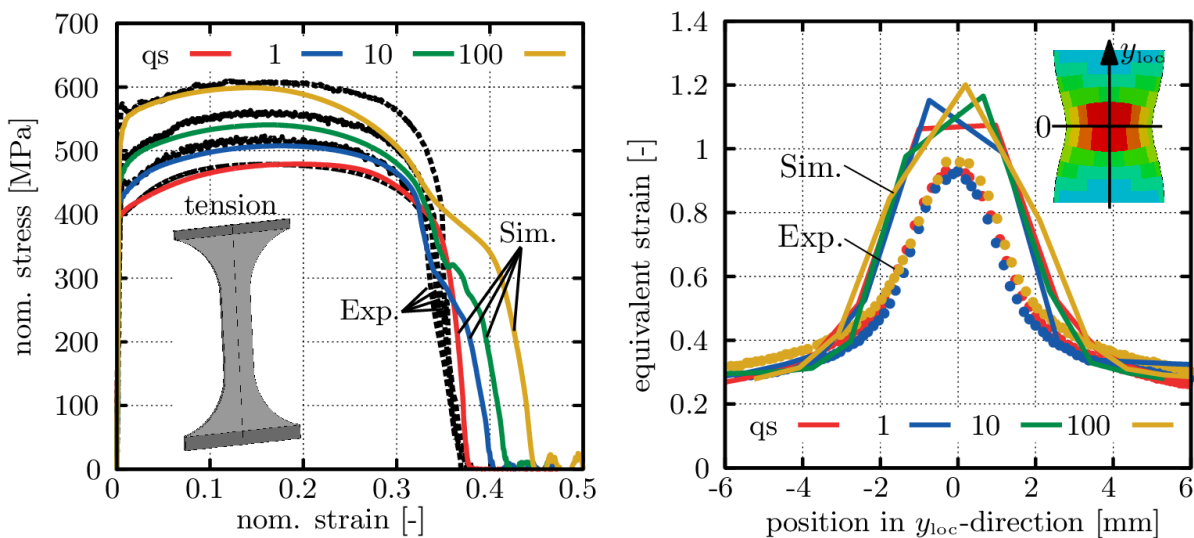


Fig.10: Comparison of simulation results to measured data from tension test with quasistatic (qs) loading up to high strain rates of 100 s⁻¹ with regard to stress-strain courses (test data from [22]) as well to equivalent strain in the necking area (test data from [23])

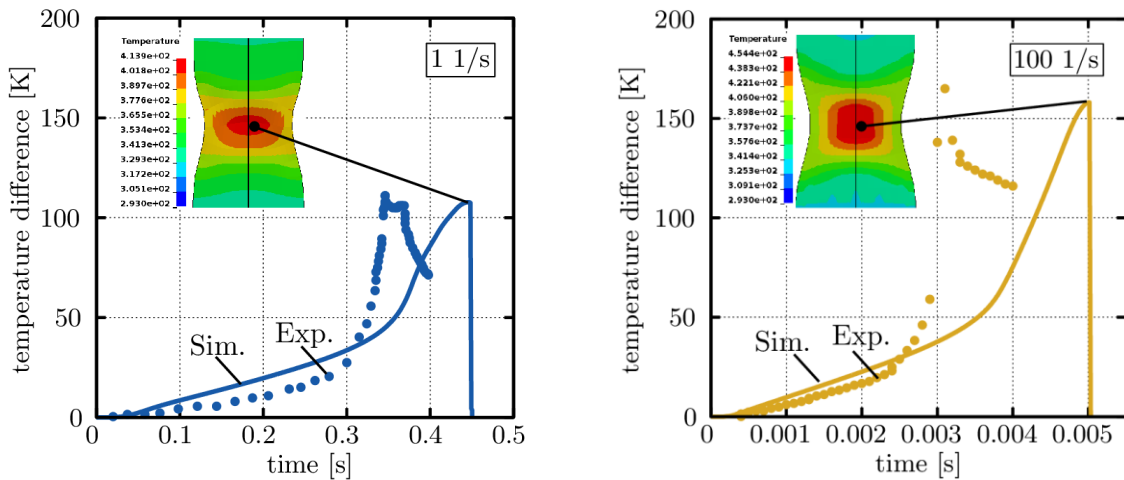


Fig.11: Comparison of simulation results to test data from tension experiments taken from [23] at medium strain rate 1 s^{-1} and high strain rate 100 s^{-1} with regard to time-temperature courses

The previous results require the consideration of thermal softening in the post-necking area for high strain rate tensile tests. Here, the dynamic failure process of other specimens is not accounted for. However, ROTH and MOHR point out the high relevance of thermal softening for high strain rate tests of uniaxial tension specimen as well as notched tensile specimen and specimens with a central hole as discussed in [25].

Considering the thermal softening, the temperature at failure is crucial to predict. Therefore, the measured temperature increase during the tensile test at the strain rate of 1 s^{-1} and 100 s^{-1} is taken from [23, p. 146] and compared to the simulation results—see Fig. 11. The temperature of both, experiment and simulation, is evaluated in the centre of the necking area, where the highest temperature rise is observed. Due to an offset in the experimentally recorded time-temperature course, the time interval of test data is shifted to the start of loading in order to achieve a comparable time scale—see also [23, p. 146]. The difference between the failure strain of the simulation and the test (see Fig. 10) causes a significant delay of the time-temperature course for the simulation compared to the measured values (see Fig. 11). However, the predicted temperature at failure coincides very well with the measured temperature data. Moreover, the minor temperature increase in the pre-necking area as well as the high temperature rise in the post-necking area is apparent in the test data and in the simulation.

Table 1: Identified model parameters for the high strength steel HX340LAD (ZStE340)

elasticity	E	420000.0 N/mm ²	Q_E	$3.6865 \cdot 10^{-4}$ 1/K	θ_E	293.0 K	ν	0.3
initial yield stress	κ_0	767.37 N/mm ²	Q_{κ_0}	$5.0867 \cdot 10^{-4}$ 1/K	θ_{κ_0}	293.0 K		
isotropic hardening	E_κ	1450.59 N/mm ²	E^∞	145.06 N/mm ²	κ^∞	215.3691 N/mm ²		
	$\alpha_{\kappa\theta}$	0.0169 1/K	θ_0	314.0 K	$\alpha_{\kappa\dot{E}}$	0.2482 1/K	\dot{E}_0	$0.0239 \frac{1}{\text{s}}$
strain rate sensitivity	η	$9.9998 \cdot 10^6$ s	m	4.0684	D_0	1.0 N/mm ²		

5 Summary

The high strength steel alloy HX340LAD (ZStE340) is investigated under quasistatic tension and shear as well as dynamic tensile loading. A thermo-viscoplastic material model is presented to capture the temperature and strain rate dependent material characteristics under dynamic loading conditions. The post-critical material behaviour is considered by a nonlocal ductile damage approach. The model parameters are identified and verified by means of the test data for the stress-strain courses as well as for the local strain distribution and the time-temperature course prior to failure. The simulated results exhibit a close agreement to the measured values. Thus, the prediction capability of the applied material model is excellent.

References

- [1] Matzenmiller, A. and Bröcker, C.: Modeling and Simulation of Coupled Thermoplastic and Thermoviscous Structuring and Forming Processes. In: H. J. Maier, K. Steinhoff and B. Svendsen (editors): "Functionally Graded Materials in Industrial Mass Production", Auerbach, Verlag Wissenschaftliche Scripten, 235–250 2009. http://www.ifm.maschinenbau.uni-kassel.de/%7Eamat/publikationen/geschuetzt/Matzenmiller-2009-Modeling_and_Simulation_of_Coupled_Thermoplastic_and_Thermoviscous_Structuring_and_Forming_Processes.pdf
- [2] Bröcker, C. and Matzenmiller, A.: "An enhanced concept of rheological models to represent nonlinear thermoviscoplasticity and its energy storage behaviour". Continuum Mechanics and Thermodynamics, vol. 25, 2013, pp. 749–778.
- [3] Bröcker, C. and Matzenmiller, A.: "An enhanced concept of rheological models to represent nonlinear thermoviscoplasticity and its energy storage behavior, part 2: spatial generalization for small strains". Continuum Mechanics and Thermodynamics, vol. 27, 2015, pp. 325–347.
- [4] Matzenmiller, A. and Bröcker, C.: "Thermo-mechanically coupled FE analysis and sensitivity study of simultaneous hot/cold forging process with local inductive heating and cooling", International Journal of Material Forming, vol. 5, 2012, pp. 275–300.
- [5] Matzenmiller, A., Bröcker, C. and Gerlach, S.: "FE-Analysis of Simultaneous Hot/Cold Forging", Steel Research Int., vol. 80, 2009, pp. 130–136.
- [6] Taylor, G. I. and Quinney, H.: "The latent energy remaining in a metal after cold working", Proc. Roy. Soc. of London, A: Mathematical, Physical and Engineering Sciences, vol. 143, 1934, pp. 307–326.
- [7] Bröcker, C. and Matzenmiller, A.: A thermoviscoplastic model with damage for simultaneous hot/cold forging analysis, In: E. Onate, D. Owen, D. Peric und B. Suarez: "Proceedings of 12th International Conference on Computational Plasticity – Fundamentals and Applications" (COMPLAS XII), International Center for Numerical Methods in Engineering, Barcelona, 2013. http://www.ifm.maschinenbau.uni-kassel.de/%7Eamat/publikationen/oefentlich/Broecker-A_THERMOVISCOPLASTIC_MODEL_WITH_DAMAGE_FOR_SIMULTANEOUS_HOT%2%81%84COLD_FORGING_ANALYSIS.pdf
- [8] Bröcker, C. and Matzenmiller, A.: "On the generalization of uniaxial thermoviscoplasticity with damage to finite deformations based on enhanced rheological models", Tech. Mechanik, vol. 34, 2014, pp. 142–165.
- [9] Szczepaniak, A., Bröcker, C. and Matzenmiller, A.: "Implementierung eines Thermoviskoplastizitätsmodells mit Schädigung für die simultane Kalt-/Warmumformung", LS-DYNA Forum, Bamberg, 2014. https://www.dynamore.de/de/download/papers/2014-ls-dyna-forum/documents/prozesssimulation-iv/implementierung-eines-thermoviskoplastizitaetsmodells-mit-schaedigung-fuer-die-simultane-kalt-warmumformung/at_download/file
- [10] Matzenmiller, A., Nahrman, M. and Kühlmeyer, P.: "Evaluation of different thermo-viscoplastic material models under simultaneous hot/cold forging conditions", 11. European LS-DYNA Conf., Salzburg, 2017. https://www.dynalook.com/conferences/11th-european-ls-dyna-conference/process-miscellaneous/evaluation-of-different-thermo-viscoplastic-material-models-under-simultaneous-hot-cold-forging-conditions/@_@download/file/02_Nahrman_Universitaet_Kassel.pdf
- [11] Lemaitre, J.: "A continuous damage mechanics model for ductile fracture", Journal of Engineering Materials and Technology vol. 107, 1985, pp. 83–89.
- [12] Lemaitre, J.: "A Course on Damage Mechanics", Springer-Verlag Berlin Heidelberg, 1996.
- [13] Johnson, G. R. and Cook, W. H.: "Fracture characteristics of three metals subjected to various strains, strain rates, temperatures and pressures", Engineering Fracture Mechanics, vol. 21, 1985, pp. 31–48.
- [14] Bao, Y. and Wierzbicki, T.: "On fracture locus in the equivalent strain and stress triaxiality space", International Journal of Material Science, vol. 46, 2004, pp. 81–98.
- [15] Bai, Y. and Wierzbicki, T.: "A new model of metal plasticity and fracture with pressure and Lode dependence", International Journal of Plasticity, vol. 24, 2008, pp. 1071–1096.
- [16] Sun, D.-Z., Andrieux, F. and Feucht, M.: "Damage modelling of a TRIP steel for integrated simulation from deep drawing to crash", 7. European LS-DYNA Conference, Salzburg, 2009. [\[pdf\]](#)
- [17] Pijaudier-Cabot, G. and Bazant, P.: "Nonlocal Damage Theory", Journal of Engineering Mechanics, vol. 113, 1987, pp. 1512–1533.
- [18] Wisselink, H. H. and Huetink, J.: "Modelling of ductile failure in metal forming", 7. European LS-DYNA Conference, Salzburg, 2009. [\[pdf\]](#)
- [19] Ahad, F. R., Enakoutsa, K., Solanki, K. N., and Bammann, D. J.: "Nonlocal modeling in high-velocity impact failure of 6061-T6 aluminum", International Journal of Plasticity, vol. 55, 2014, pp. 108–132.
- [20] Schwer, L.: "A Brief Look at *MAT_NONLOCAL: A Possible Cure for Erosion Illness?", 11. International LS-DYNA Conference, Dearborn, USA, 2010. [\[pdf\]](#)
- [21] Engelen, R. A. B.: "Plasticity-induced damage in metals : nonlocal modelling at finite strains", PhD thesis, Technische Universiteit Eindhoven, 2005. [\[pdf\]](#)
- [22] Meschut, G., Hahn, O., Hein, D., Matzenmiller, A. and Nelson, A.: "Experimentelle und numerische Untersuchungen des Crashverhaltens hybridgefügtter Verbindungen", FOSTA report no. 958, 2015.
- [23] Trondl, A., Klitschke, S., Böhme, W. and Sun, D.-Z.: "Verformungs- und Versagensverhalten von Stählen für den Automobilbau unter crashartiger mehrachsiger Belastung", Forschungsvereinigung Automobiltechnik e.V., Behrenstraße 35, 10117 Berlin, FAT report no. 283, 2015. [\[pdf\]](#)
- [24] Meschut, G., Gerkens, M.: "Entwicklung einer Methode zum Nachweis der Einsetzbarkeit des Hochgeschwindigkeits-Bolzensetzen unter Berücksichtigung der Bauteileigenschaften", Europäische Forschungsgesellschaft für Blechverarbeitung e.V., Lothringer Str. 1, 30559 Hannover, report no. 455, 2017.
- [25] Roth, C. C. and Mohr, D.: "Effect of strain rate on ductile fracture initiation in advanced high strength steel sheets: Experiment and modeling", International Journal of Plasticity, vol. 56, 2014, pp. 19–44.
- [26] Stander, N., Roux, W., Basudhar, A., Eggleston, T., Goel, T. and Craig, K.: "LS-OPT® User's Manual – A design optimization and probabilistic analysis tool for the engineering analyst", version 5.2, 2015. [\[pdf\]](#)